ELSEVIER

Soil Dynamics and Earthquake Engineering 23 (2003) 483–495

SOIL DYNAMICS AND EARTHQUAKE ENGINEERING

www.elsevier.com/locate/soildyn

Damping/global energy balance in FE model of bridge foundation lateral response

R. Dobry[a,*], A. Pecker[b], G. Mavroeidis[c], M. Zeghal[a], B. Gohl[d], D. Yang[e]

[a]*Department of Civil and Environmental Engineering, Rensselaer Polytechnic Institute, JEC 4049, Troy, NY 12180, USA*
[b]*Geodynamique et Structure, 157 Rue des Blains, 92220 Bagneux, France*
[c]*Department of Civil, Structural and Environmental Engineering, State University of New York at Buffalo, 212 Ketter Hall, Buffalo, NY 14260, USA*
[d]*Pacific Geodynamics, Inc. 14 Sherwood Place, Delta, BC, Canada V4L 2C7*
[e]*Buckland & Taylor Ltd, 101-788 Harbourside Drive, North Vancouver, BC, Canada V7P 3R7*

Accepted 22 March 2003

Abstract

A global energy analysis is presented of three static unloading–reloading foundation lateral loading cycles, calculated using the nonlinear finite element (FE) program DYNAFLOW. This simulates seismic action on an offshore pier foundation in the Rion-Antirion Bridge in Greece, located in deep-sea water (65 m). A cyclic horizontal force is applied at a height of 30 m to a rigid raft 78 m in width placed on the surface of an idealized 2-layer soil profile consisting of a 3.5 m man-made gravel layer over soft deep natural clay, with elastic vertical steel inclusions reinforcing the soil. Results of the two-dimensional FE run are used for the energy analysis. It is verified that for the three cycles, the sum of energies associated with the external forces and moments, mostly dissipated through hysteresis loops, is about equal to the sum of the total internal energies dissipated or stored in the system. For the smaller loops almost all energy is dissipated in the soil, while for the largest loop about half of the energy is dissipated by horizontal sliding at the raft-soil interface. Global damping ratios obtained from the areas of the horizontal and rocking moment hysteresis loops are about double of those computed from the corresponding static backbone curves using the Masing criterion.

Keywords: Energy balance; Damping; Bridge foundation; Rion-Antirion project; Finite element modeling

1. Introduction

The Rion-Antirion bridge project is a contract granted by the Greek Government to a consortium led by the French company Vinci Construction. It is located in Greece, near Patras, and will constitute a fixed link between the Peloponnese Peninsula and the Continent across the western end of the Corinth Gulf (Fig. 1). The solution adopted for this bridge is a multiple span cable-stayed bridge with four main piers. Each of the three central spans is 560 m long; these central spans are extended by two flanking spans 286 m long each. The total length of the bridge including approach viaducts is approximately 3.5 km. The bridge is located in a highly seismic area and had to be designed for a number of severe environmental conditions [1,2]:

- the foundation soils are soft alluvial deposits (mostly silty clays and clayey silts) extending to depths greater than 500 m. Subsurface exploration to depths up to 100 m, using various offshore exploratory methods, determined that these soils have rather poor mechanical characteristics. While the clays are overconsolidated at shallow elevations, their overconsolidation ratio decreases rapidly with depth and it is only about 1.3 at a depth of 50 m below the sea bed. The undrained shear strength increases slowly with depth from approximately 30–50 kPa at the ground surface (sea bed) to 100–150 kPa at 50 m depth; the shear wave velocity increases from 100–150 m/s at the ground surface to 350–400 m/s at 100 m depth;

* Corresponding author. Tel.: +1-518-276-6934; fax: +1-518-276-4833.
E-mail addresses: dobryr@rpi.edu (R. Dobry), alain.pecker@geodynamique.com (A. Pecker), gm25@eng.buffalo.edu (G. Mavroeidis), zeghal@rpi.edu (M. Zeghal), pgigohl@telus.net (B. Gohl), dyang@b-t.com (D. Yang).

0267-7261/03/$ - see front matter © 2003 Elsevier Ltd. All rights reserved.
doi:10.1016/S0267-7261(03)00050-2

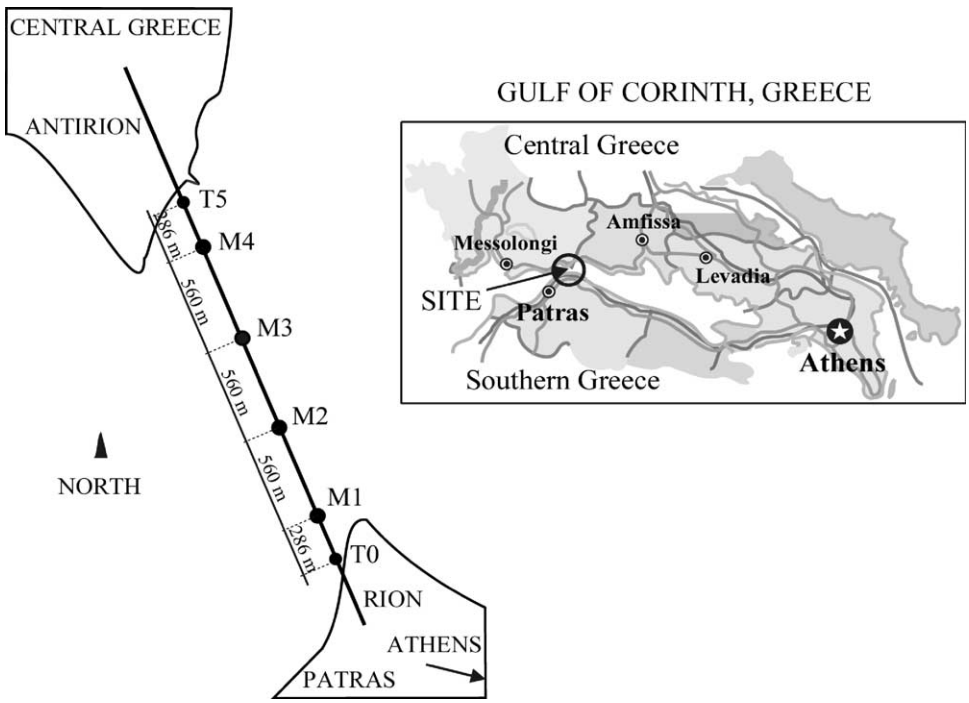

Fig. 1. Rion-Antirion Bridge location plan.

- the water depth in the middle of the strait reaches 65 m;
- the seismic design motion, obtained from a 2000-year return period, corresponds to an earthquake of magnitude 7.0 and peak ground surface acceleration of 0.48*g*. The associated 5% damped response spectrum has a plateau at 1.2*g* for a range of periods extending from 0.2 to 1.1 s. At a period of 2 s the spectral acceleration is still equal to 0.62*g* (Fig. 2); and
- the bridge must accommodate a 2 m differential tectonic displacement in any direction and between any two piers.

In order to alleviate potential damage to the structure due to the above adverse conditions and to carry the large earthquake forces imposed on each pier foundation (i.e. shear horizontal force of the order of 500 MN and overturning moment of the order of 18,000 MN m for a vertical buoyant pier weight of 750 MN), an innovative foundation design concept was adopted. It consists of a gravity caisson (i.e. 90 m in diameter at the sea bed level), resting on top of the natural ground after reinforcing the soil [3]. The ground reinforcement is composed of steel pipes, 2 m in diameter, 20 mm wall thickness, and 25–30 m long driven in a grid of 7 m × 7 m below and outside the foundation, covering a circular area of 13,300 m^2. The total number of inclusions planned under each foundation and considered at the time of the analyses reported herein was of the order of 270. (These figures just listed correspond to the preliminary scheme studied in this paper. Further development of the final design lead to smaller numbers of inclusions which varied depending on the geotechnical conditions at each pier location: 130–170 inclusions covering a circular area ranging between 6500 and 8500 m^2).

An additional enhancement of the safety of the foundation is provided by overlaying a 2.8 m-thick gravel bed layer on top of the natural clay, with the steel inclusions penetrating the gravel layer but not reaching the ground surface. Thus, the inclusion heads have no structural connection with the foundation raft (Figs. 3 and 6). This concept (i.e. inclusions plus gravel layer) is aimed at enforcing a capacity seismic design philosophy for the foundation [4]. The gravel layer plays the role of a 'plastic hinge', where inelastic deformation and dissipation take place in the horizontal direction, while the 'over-strength'

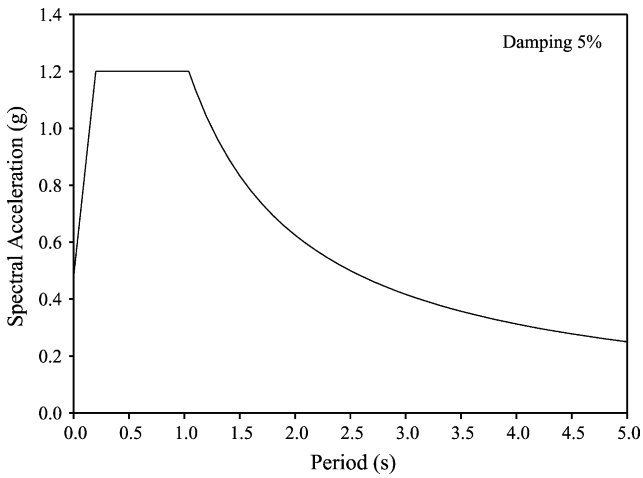

Fig. 2. Design response spectrum.

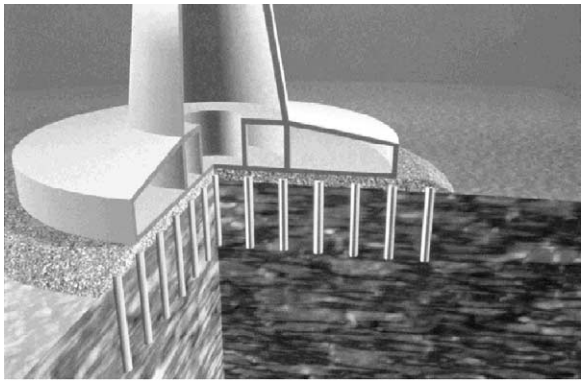

Fig. 3. Foundation cross-section of a bridge pier, showing gravel layer, natural clay, and steel pipe inclusions placed to reinforce the clay.

provided by the ground steel reinforcement prevents the development of deep-seated rotational failure mechanisms. Numerical analyses as well as centrifuge model tests conducted for the project have shown that the 'failure' mode would indeed be pure sliding at the gravel-foundation interface. This 'failure mechanism' and accompanying displacements can be accommodated by the bridge, which is designed for much larger tectonic displacements than the permanent displacements that may be induced by the shaking.

The implementation of this innovative foundation concept required the development of several numerical tools, as well as physical model tests and a large number of analyses to validate the concept, check the results and implement the design. The pseudo-static bearing capacity of the foundation subjected to combined vertical force–horizontal shear force–overturning moment loading was evaluated with a limit analysis method based on the yield design theory [5,6]. These limit analyses were supplemented by nonlinear finite element (FE) calculations and centrifuge model tests, which both validated the concept and confirmed the values of the ultimate foundation load combinations. The FE analyses and centrifuge tests also provided the parameters required to assess the foundation displacements as a function of the applied loads, as these displacements could not be evaluated by the yield design theory.

For the dynamic seismic analyses of the whole bridge, it was not realistic to contemplate a global model including soil, inclusions and structure. Therefore, a simplified rheological model representing the soil-inclusions–structure interaction [7], for each foundation degree of freedom (i.e. vertical, horizontal and rocking), was developed for use in the numerous required parametric analyses. This simplified model has been checked with several independent tools, such as 2D nonlinear dynamic FE analyses of an isolated pier including the foundation soil mass, inclusions and pier footing; as well as displacements measured during cyclic loading of centrifuge models.

The objective of this paper is to present one aspect of the validation of the rheological model based on pseudo-static cyclic FE analyses. The analyses presented herein were used to identify the elements of the foundation system contributing to the energy dissipation mechanism and to validate its implementation in the rheological model. This study was jointly conducted by the design team represented by one of the authors (A.P.) and by the Checker's team acting on behalf of the design Checker, Buckland and Taylor Ltd. of Canada.

2. Rheological model

The model is based on the concept of substructuring a semi-infinite soil mass [8]. As shown schematically in Fig. 4, the soil volume is conceptually divided in two regions:

- a near-field region, which encompasses all nonlinearities related to the interaction between soil, structure and reinforcing inclusions. This includes nonlinearities generated within the soil and associated with its stress–strain constitutive relation, as well as foundation uplift and sliding at soil-foundation and soil-inclusion interfaces. In the near field, the energy dissipation mechanism is assumed to be predominantly hysteretic and rate independent; and
- a far-field region, where there is much less nonlinearity, with essentially all of it related to seismic wave propagation in the soil. As the energy dissipation in the far field is associated exclusively with such wave propagation (radiation damping), the energy dissipation mechanism is assumed to be predominantly viscous.

For each degree of freedom of the foundation (i.e. vertical, torsional, horizontal, rocking), the semi-infinite soil mass (Fig. 4) may be approximated conceptually by the simplified rheological model of Fig. 5. In this mechanical approximation, the soil mass is replaced by an assemblage of springs, viscous dashpots, and sliders connected to the base of the foundation. Only the horizontal and rocking degrees of freedom are considered herein. For these two degrees of freedom of the foundation, the parameters of the model in Fig. 5 were determined, for initial loading, from static monotonic nonlinear FE analyses conducted up to failure of the foundation. For unloading–reloading horizontal and rocking foundation response, the simple Masing criterion [9] was assumed in the bridge project; as shown by Iwan [10], a combination of springs and sliders such as used in the scheme of Fig. 5 for the near field produces hysteresis loops in accordance with the Masing criterion. That is, it is assumed that the energy dissipation mechanism in the near-field region obeys Masing's criterion and rules as commonly assumed in soil constitutive modeling [11].

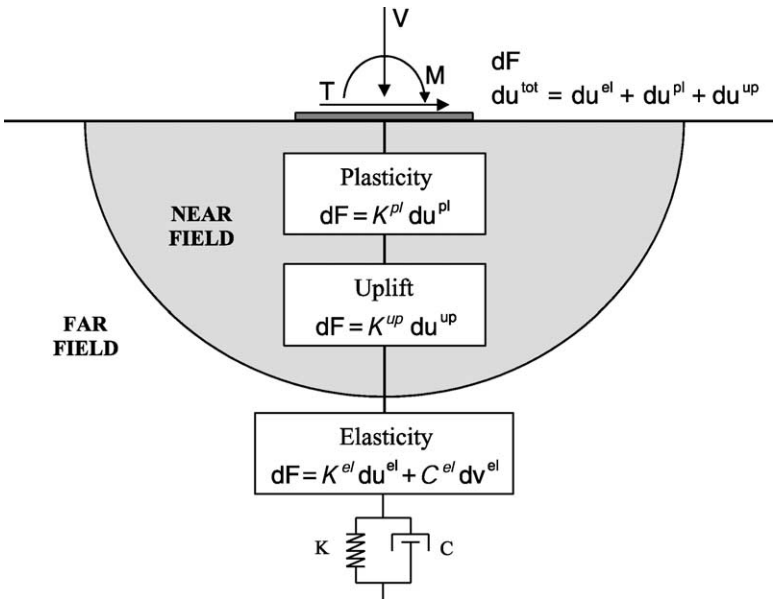

Fig. 4. Substructure dynamic model of soil plus inclusions under the bridge foundation.

The determination of loading–unloading–reloading horizontal and rocking foundation response from the static nonlinear FE analyses, in conjunction with the assumed Masing criterion, completely defines the global behavior of the foundation connected to the springs and sliders of Fig. 5 including both near field and far field. (Only the far-field viscous dashpot C_0 is not covered, which should have negligible influence on horizontal and rocking responses for the range of amplitudes and frequencies of interest). However, the assumed validity of Masing criterion for cyclic response and energy dissipation under the foundation was identified by the Checker's team to be a critical modeling issue, which needed further clarification and validation.

While the model can be refined to include the coupling between the various degrees of freedom of the foundation [8], the specific rheological model implementation for the design studies of the Rion-Antirion Bridge assumed that all foundation degrees of freedom are uncoupled, which represents a significant simplification. The uncoupled model used in this paper was accurate enough from an engineering standpoint and was extensively used for the structural seismic analyses of the bridge.

3. Two-dimensional finite element modeling

A two-dimensional FE model was developed for the soil-foundation system including soil, inclusions, gravel bed layer and foundation raft [12]. This FE model was used to calibrate the simplified rheological model of Fig. 5 for lateral seismic loading, and to clarify the associated low-frequency, near-field energy dissipation mechanisms in the foundation system.

Figure 6 sketches basic aspects of the raft-soil-inclusions 2D FE model used for these static loading–unloading–reloading analyses, while Fig. 8 illustrates the 100 m × 400 m overall dimensions of the corresponding FE mesh. The undrained shear strength profile shown for the natural clay in Fig. 6 does not correspond to the actual profile prevailing at any foundation location. Rather, it is a simplified profile derived from the soil investigations along the bridge. Otherwise, Fig. 6 reflects foundation design decisions: a foundation raft on top of the man-made gravel layer of $\phi = 40°$ where the inclusion heads are embedded. As the 2D FE run reported herein was done early in the project, some of the parameters used in the calculations are

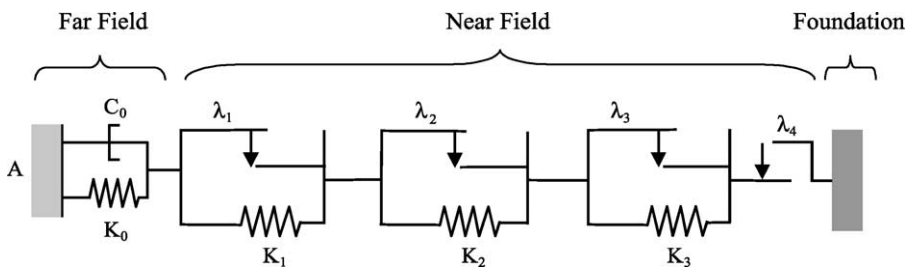

Fig. 5. Simplified dynamic rheological model of foundation-soil-inclusions system.

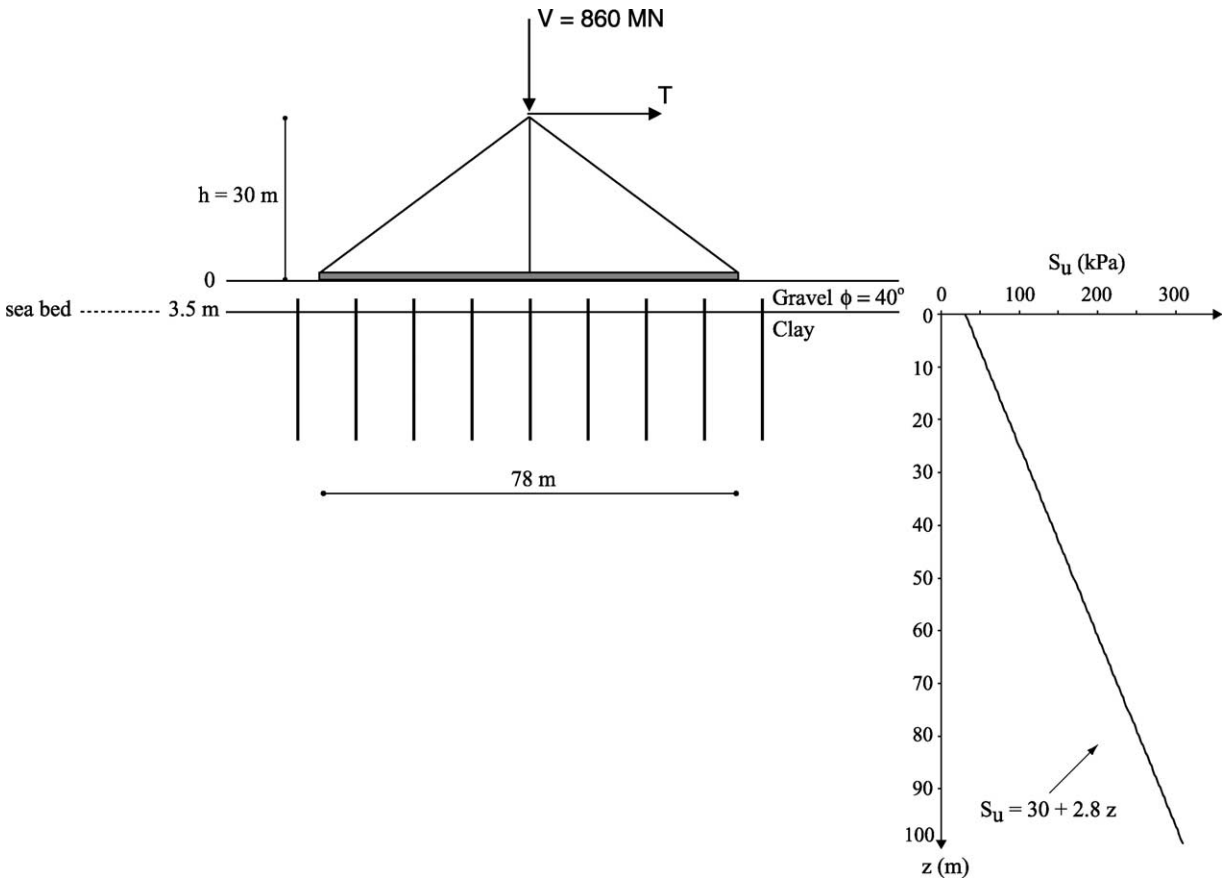

Fig. 6. Basic aspects of the raft-soil-inclusions 2D FE model.

different from those adopted in the final design of the bridge foundation.

3.1. Soil constitutive model

Consistent with Figs. 4 and 5, the nonlinear natural and man-made soil behavior is modeled with elastoplastic constitutive relationships. A kinematic hardening rule is used along with the multi-yield surface technique originally developed by Prevost [13,14]. In this technique, a collection of nested yield surfaces allows for adjustment of the kinematic hardening rule to any kind of experimental hardening law obtained in monotonic triaxial or simple shear tests. The initial positions and sizes of the yield surfaces reflect the past stress–strain history of the soil. During loading and unloading–reloading, the yield surfaces are allowed to move in stress space to reflect the partial yielding of the material. The outermost yield surface represents the failure surface and is fixed in stress space. The behavior inside the innermost surface is elastic and isotropic [13].

The objective of the FE analysis is to represent the nonlinear response of the foundation under seismic loading, which is rapid enough so that no drainage is possible in the clay. Therefore, Von Mises yield and failure criteria (i.e. circular cylinders in principal stress space), are used for the natural clay deposit. Thus, the constitutive model of the clay is completely characterized by [13]:

- the elastic parameters (shear modulus, G, and bulk modulus, B); and
- the plastic parameters (undrained shear strength, S_u, and stress–strain relationship under undrained monotonic triaxial or simple shear experiment).

These parameters were idealized as functions of depth z below the original ground surface (sea bed level), based on the results of soil investigations including in situ cone penetration and shear wave velocity measurements as well as laboratory tests. For the elastic shear modulus, $G = 20z^{0.65}$, where G is in MPa and z in m. To model a constant volume condition under undrained loading, a large bulk modulus, B, was assigned to the soil, equivalent to assigning a Poisson's ratio approaching 0.5 in terms of total stresses. The undrained shear strength is specified as $S_u = 30 + 2.8z$, where S_u is in kPa and z in m (Fig. 6). The sizes and positions of the nested yield cylindrical surfaces which govern the hardening behavior, were determined from the stress–strain curve measured in a constant-volume

monotonic simple shear test, and further verified at small strains by resonant column testing (Fig. 7).

To fulfill its role as a 'plastic hinge', the gravel layer under the foundation raft must provide a limited and well defined shear capacity at the soil-foundation interface; this can be assured if the material remains drained (i.e. pervious enough to dissipate rapidly during the seismic shaking any pore pressure induced by the combined cyclic and static loads). This condition is assumed in the model, and the gravel layer is characterized in terms of effective stresses, with Drucker–Prager yield and failure criteria that approximate the usual Mohr–Coulomb failure law typically used for cohesionless soils in geotechnical engineering practice. The flow rule is non-associative and reflects the change from contractive to dilative behavior as the stress point crosses the phase transformation line, defined by the 'characteristic' friction angle. The model is built on the same concept of nested yield surfaces with kinematic hardening already described for the clay layer, but now with failure surface and nested yield surfaces being circular cones in effective stress space [14].

The constitutive model of the gravel is completely defined by:

- the elastic parameters (G and B); and
- the plastic parameters (friction angle, characteristic friction angle, stress–strain relationship under

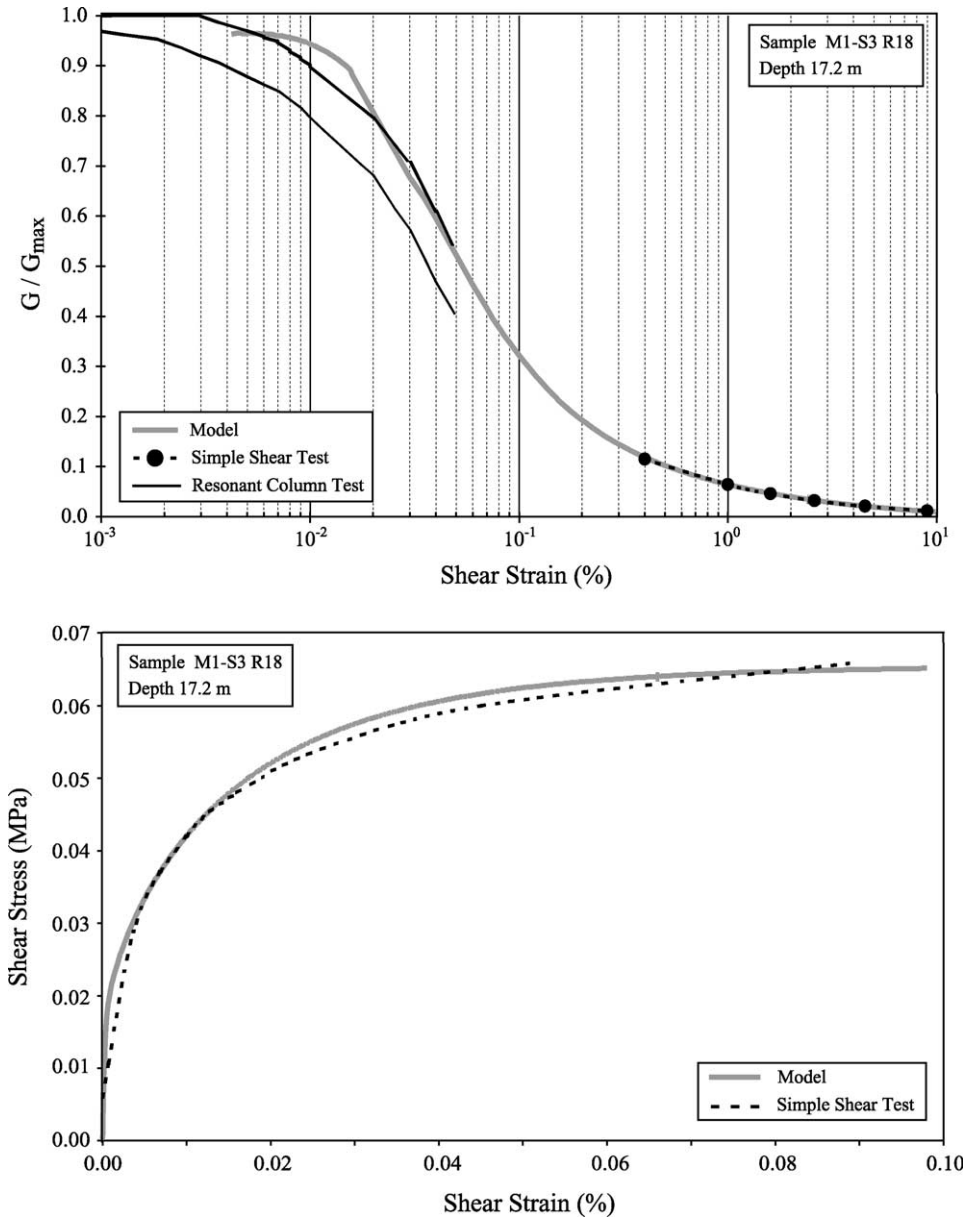

Fig. 7. Comparison between constitutive model predictions for the clay and experimental results from constant-volume simple shear and resonant column testing.

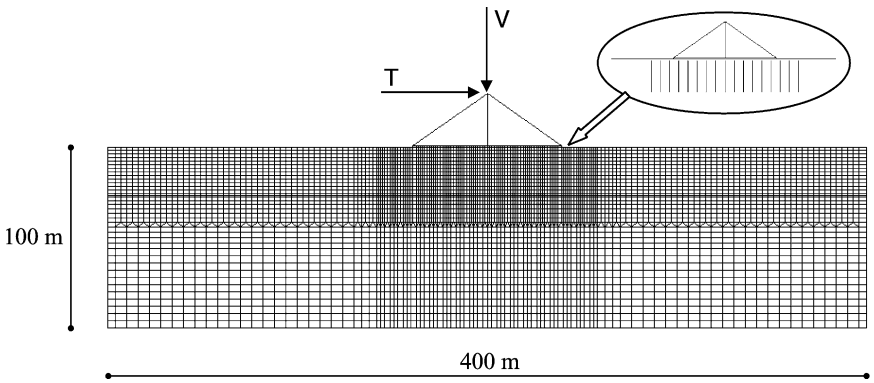

Fig. 8. Global finite element mesh for the 2D FE run using program DYNAFLOW.

monotonic triaxial compression test, and dilation parameter which governs the rate of variation of the plastic volumetric strain).

These elastic and plastic parameters of the gravel layer are associated with the solid phase, and thus correspond to drained loading and effective stresses, in contrast to the clay which is characterized in terms of total stresses.

The elastic parameters of the gravel are defined by the following expressions: $G = 2000p_a(\sigma'_m/p_a)^{0.5}$, and $B = 2700p_a(\sigma'_m/p_a)^{0.5}$; where σ'_m is the mean effective stress and p_a is the atmospheric pressure used as a normalizing factor. A friction angle of 40° is used for the gravel, as well as a characteristic friction angle of 33°. The dilational parameter is chosen equal to 0.3 [15]; numerical simulations have shown that the results are rather insensitive to this dilational parameter.

3.2. Finite element model

The 2D FE analyses were performed with computer program DYNAFLOW [16], as reported by Geodynamique et Structure [12]. Therefore, the calculations correspond to a 1 m-wide slice of the actual 3D system. The mechanical properties of the inclusions were divided by their transverse spacing, and an equivalent width was computed for the foundation. The global FE mesh is presented in Fig. 8. The overall dimensions are 400 m in width and 100 m in depth; the soil layer was divided into 35 sublayers. The inclusions were modeled as elastic beams capable of deforming in both bending and shear; the length of each inclusion was 25 m, with 2 m in the gravel layer and 23 m in the clay. A uniform spacing of 7 m between inclusions was used both below and outside the foundation raft. Each inclusion was modeled with 13 beam elements. The foundation raft (90 m in diameter) was represented by an equivalent rectangular foundation with an in plane width of 78 m (Fig. 6) and an out-of-plane length of 82 m. These rectangular dimensions were obtained by preserving the area and area moment of inertia of the original 90 m circle.

Interface elements were introduced in the model along the inclusions and along the base of the raft. These elements represent the limited shear capacity that can be mobilized between two different media; they were modeled with elastic-perfectly plastic springs having no tensile strength. As long as the shear stress induced in the interface element is smaller than its ultimate strength, perfect bonding is enforced between both media; if tensile forces tend to develop, a gap is formed and the element no longer transmits any normal or shear force. Along the raft-gravel boundary, the ultimate strength of the interface elements was governed by Mohr–Coulomb criterion with $\phi = 40°$; along the inclusions in the clay layer, it was made equal to the soil undrained shear strength.

3.3. Loading and results of the FE analysis

The load applied to the foundation consisted of a constant vertical force, V, (i.e. buoyant weight of the pier caisson plus foundation), and variable horizontal shear force, T, and overturning rocking moment, M (Figs. 6, 8 and 9). Due to the massive, extremely stiff character of the pier caisson, the combination of shear force and overturning moment could be conveniently represented for the pseudo-static analysis by a horizontal shear force acting at an elevation h above the foundation level. This elevation corresponds to the pier mass center of gravity and is approximately equal to 30 m (Fig. 6). The validity of this assumption that $h = 30$ m constituted a reasonable average during seismic shaking was checked by independent analyses. In the FE model, the horizontal force, T, was therefore applied at an elevation $h = 30$ m to a rigid frame connected to the foundation

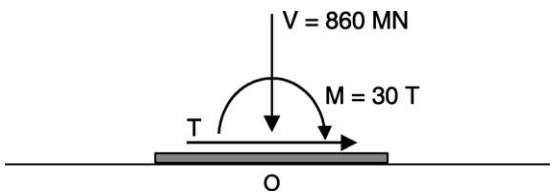

Fig. 9. External forces and moment acting on raft.

(Figs. 6 and 8). Therefore, the specific static loads applied to the foundation raft to approximate conditions during the seismic shaking are as shown in Fig. 9: a constant vertical force, $V = 860$ MN (corresponding to the weight of pier caisson plus raft), a variable horizontal force, T, and a variable rocking moment, $M = 30T$, where T is in MN and M is in MN m. (The sketch of Fig. 9: includes $V = 860$ MN corresponding to the original 3D circular foundation; in the 2D FE run sketched in Fig. 8 the loads were divided by the 82 m out-of-plane length, and thus $V = 860/82 = 10.49$ MN/m.)

The sequence of loading applied to the foundation included the following three steps:

- *Step 1*. Initialization of gravity stresses in the soil, without the structure.
- *Step 2*. Consolidation of soil by application of structure weight up to $V = 10.49$ MN/m (corresponding to 860 MN in actual foundation).
- *Step 3*. Application of cycles of horizontal force T at elevation $h = 30$ m, corresponding to simultaneous variation of T and $M = 30T$ as shown in Fig. 9.

Each step was applied incrementally. Steps 1 and 2 were conducted in drained condition (i.e. the pore fluid bulk modulus was set equal to 0 in the program), and Step 3 was run under undrained condition in the clay layer (i.e. the fluid bulk modulus was set to a high value in the program). The solution of the FE nonlinear system of equations was obtained by means of an iterative strategy including an implicit–explicit predictor–multicorrector scheme and a quasi Newton (BFGS) algorithm.

The hysteresis loops computed by the program for three increasing values of cyclic horizontal displacement of the foundation raft, u_m, are presented in Figs. 10 and 11. These values are: $u_m = 0.12, 0.34$ and 0.55 m. Fig. 10 shows the results in terms of horizontal force, T, versus horizontal displacement, u_H, and Fig. 11 presents the results of the

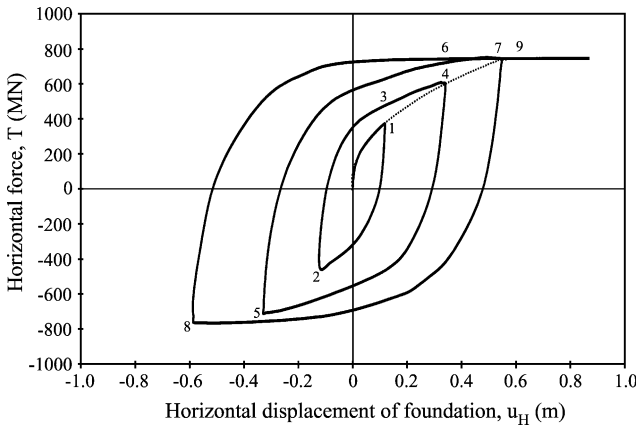

Fig. 10. Horizontal force—displacement calculation from 2D FE run.

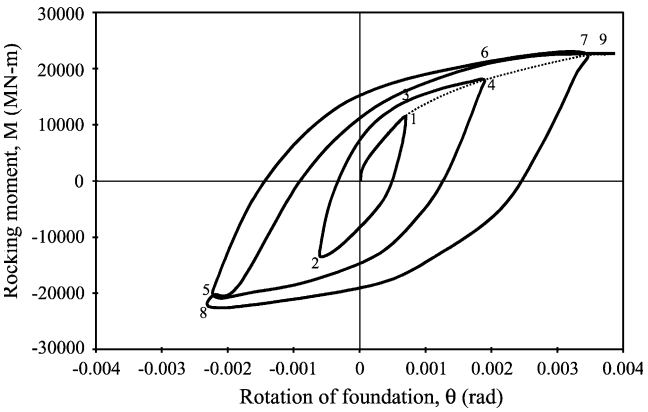

Fig. 11. Rocking moment—rotation calculation from 2D FE run.

same computer run as rocking moment, M, versus rotation angle, θ, of the raft. The loading sequence is indicated in the plots. That is, the force T was first increased monotonically from the origin to Point 1, where $u_H = u_m = 0.12$ m, then unloaded to Point 2 where $u_H = -u_m = -0.12$ m, reloaded to Point 3 where, again, $u_H = u_m = 0.12$ m, with reloading continued to Point 4 to the next larger $u_m = 0.34$ m, then unloaded to Point 5, etc. Simultaneously, the moment $M = 30T$ and rotation θ calculated by the FE program were increasing and decreasing as noted in Fig. 11 by Points 1, 2, 3, etc. That is, the values of T, u_H, M and θ at corresponding points in Figs. 10 and 11 (e.g. Point 1 in both plots), occur simultaneously in the loading–unlading–reloading sequence of the foundation system. The force and moment presented in Figs. 10 and 11 are relevant to the actual 3D foundation (i.e. numerical results of the 2D FE analyses have already been multiplied by the out-of-plane length of 82 m). Note that the loops in Figs. 10 and 11 are not necessarily closed; for example, while both Points 1 and 3 in Fig. 10 correspond to the same horizontal displacement, $u_H = u_m = 0.12$ m, the force T is higher at Point 3. The static force-displacement and moment-rotation loops calculated with 2D FE program DYNAFLOW and presented in Figs. 10 and 11, form the basis for the additional analyses and interpretations presented in this paper.

4. Global energy balance and foundation damping

A global energy and damping analysis was conducted using the results of the DYNAFLOW FE run summarized in Figs. 10 and 11 [17], in order to:

- verify that for each of the hysteresis loops, the sum of external energies associated with the three loads shown in Fig. 9, is equal to the sum of the internal energies either dissipated in the soil and at the soil-foundation interfaces, or stored elastically in the inclusions (energy conservation principle);

- provide insight into the physical sources of energy dissipation through the system, to explain the very significant damping ratios obtained from the loops in Figs. 10 and 11, and listed in Table 5
- use this insight to implement simplifications and savings in further 2D and 3D FE runs of the foundation by eliminating modeling details that do not contribute significantly to the overall foundation stiffness and damping; and
- verify the assumption that the use of the Masing criterion in dynamic nonlinear analyses of the bridge, in conjunction with the horizontal and rocking monotonic backbone curves in Figs. 10 and 11, is either realistic or conservative in that it predicts equal or less damping ratios than calculated from the corresponding loops in Figs. 10 and 11.

Sections 5 and 6 present, respectively, the theory used for this global energy analysis and the numerical results of the analysis, together with a discussion on the validity of the Masing criterion as an engineering approximation of the seismic foundation response of the Rion-Antirion Bridge.

5. Theory

The global energy conservation requirement for quasi-static loading of the foundation-soil system may be expressed as:

$$\int_v \int_\varepsilon \sigma : \mathrm{d}\varepsilon \, \mathrm{d}v = \int_s \int_\mathrm{u} \mathbf{t}\cdot\mathrm{d}\mathbf{u} \, \mathrm{d}s + \int_v \int_\mathrm{u} \mathbf{b}\cdot\mathrm{d}\mathbf{u} \, \mathrm{d}v \tag{1}$$

where σ is stress tensor, ε is strain tensor, $\mathbf{u}$ is displacement vector, $\mathbf{t}$ is external (traction) load vector applied to the boundary s, $\mathbf{b}$ is external body (i.e. gravity) force vector, and v is volume of the foundation-soil system. This equation is a corollary of the principle of virtual work, which also constitutes the basis of the FEM weak formulation of the equations of motion. In the analyses reported herein, the integrations in Eq. (1) are carried following the hysteretic unloading–reloading loop of the horizontal external load (e.g. between Points 1, 2, and 3 in Figs. 10 and 11), and hence much of the energies in Eq. (1) are dissipated energies.

The left-hand side of Eq. (1) corresponds to the internal energy dissipated in the soil or at the soil-raft or soil-inclusions interfaces, plus the elastic energy stored in the elastic inclusions. The first term at the right-hand side of Eq. (1) corresponds to the work done by the external horizontal force, T, applied at a height of 30 m above the raft (Fig. 6), which can in turn be decomposed between work done by the load T at the level of the raft plus work done by the moment $M = 30T$. Finally, the second right-hand side term of Eq. (1) is the work done by the gravitational loads during vertical displacements. These vertical loads correspond to the weights of the pier, raft, soil and inclusion elements. In what follows, each of the general terms in Eq. (1) is expressed as a sum of contributions specific to the problem at hand (i.e. 2D static FE run using program DYNAFLOW, summarized in Figs. 10 and 11). For the 2D FE model, the volume and surface integrations of Eq. (1) are reduced, respectively, to surface and line integrations. The results of these integrations are then multiplied by the transverse length of 82 m (perpendicular to the FE model), to obtain the corresponding energies in the 3D system.

The total work done by the internal forces (left-hand side of Eq. (1)) is labeled $\sum W_\mathrm{i}$ and can be decomposed as follows:

$$\sum W_\mathrm{i} = \int_v \int_\varepsilon \sigma : \mathrm{d}\varepsilon \, \mathrm{d}v$$

$$= W_\mathrm{g} + W_\mathrm{c} + W_\mathrm{ier} + W_\mathrm{iei} + W_\mathrm{el} + W_\mathrm{tip} \tag{2}$$

For the two-dimensional strain solution of the foundation-soil system, and a typical soil (gravel or clay) element:

$$\sigma : \mathrm{d}\varepsilon = \sigma_{xx} d\varepsilon_{xx} + \sigma_{yy} d\varepsilon_{yy} + \tau_{xy} \mathrm{d}\gamma_{xy} \tag{3}$$

where (x, y) is a system of Cartesian coordinates, typically vertical and horizontal.

For the foundation-soil system, $\sum W_\mathrm{i}$ in Eq. (2) comprises:

- $W_\mathrm{g} = \int_{v_\mathrm{g}} \int_\varepsilon \sigma : \mathrm{d}\varepsilon \mathrm{d}v_\mathrm{g}$; work done by internal forces (stresses) by soil elements within the gravel layer (of volume v_g), calculated with Eq. (3).
- $W_\mathrm{c} = \int_{v_\mathrm{c}} \int_\varepsilon \sigma : \mathrm{d}\varepsilon \mathrm{d}v_\mathrm{c}$; work done by internal forces (stresses) by soil elements within the clay layer (of volume v_c), calculated with Eq. (3).
- $W_\mathrm{ier} = \int_{s_\mathrm{r}} \int_\varepsilon \sigma : \mathrm{d}\varepsilon \mathrm{d}s_\mathrm{r}$; work done by internal forces at the interface between the raft and the underlying soil of surface s_r. In terms of normal and tangential components this work may be expressed as $W_\mathrm{ier} = \int_{s_\mathrm{r}} \int_\varepsilon (\sigma_\mathrm{n} \mathrm{d}\varepsilon_\mathrm{n} + \tau \, \mathrm{d}\gamma) \mathrm{d}s_\mathrm{r}$, with σ_n and τ interpreted as the normal and tangential interface forces, and $\mathrm{d}\varepsilon_\mathrm{n}$ and $\mathrm{d}\gamma$ interpreted as the normal and tangential interface relative displacements across the interface element. As the normal relative displacement along the interface should generally be equal to zero ($\mathrm{d}\varepsilon_n = 0$), it is expected that only the term $\tau \mathrm{d}\gamma$ contributes to W_ier. When uplifting occurs and $d\varepsilon_n$ is different from zero, the normal force $\sigma_\mathrm{n} = 0$, and again only the term $\tau \mathrm{d}\gamma$ should contribute to W_ier.
- $W_\mathrm{iei} = \int_{s_\mathrm{i}} \int_\varepsilon \sigma : \mathrm{d}\varepsilon \mathrm{d}s_\mathrm{i}$; work done by internal forces at the interfaces between the inclusions and the surrounding soil (of surface s_i). The considerations and analytical expressions for the calculation of W_ier apply for W_iei as well.
- W_el; work done by internal forces of the elastic inclusions. In view of the elasticity of the inclusions (i.e. the behavior is not path dependent), the work done by the internal force is equal to the difference in strain

Table 1
External energy input

Loop	u_m (m)	W_T (MN m)	W_M (MN m)	W_V (MN m)	W_{BF} (MN m)	ΣW_e (MN m)
123	0.12	153.6	19.4	48.9[a]	NC	173.0 (221.9)
456	0.34	718.9	105.6	115.7[a]	NC	824.5 (940.2)
789	0.55	1487.5	157.8	130.1[a]	NC	1645.3 (1775.4)

NC: not computed.
[a] Uncertain estimate

energy stored in the inclusions at the end and the beginning of the loading cycle: $W_{el} = \int_v (\sigma_f : \varepsilon_f - \sigma_i : \varepsilon_i) dv$ (where σ_i and σ_f are the initial and final stress tensors, and ε_i and ε_f are the corresponding strain tensors).

- $W_{tip} = \int_{s_{tip}} \int_{\varepsilon} \sigma : d\varepsilon ds_{tip}$; work done by internal forces at the interfaces between the tips of the inclusions and the surrounding soil (of surface s_{tip}).

The two terms in the right hand side of Eq. (1) are the work done by the external surface and body forces (**t** and **b** respectively), acting on the foundation-soil system, and their sum is labeled $\sum W_e$:

$$\sum W_e = \int_s \int_u \mathbf{t}\cdot d\mathbf{u}\, ds + \int_v \int_u \mathbf{b}\cdot d\mathbf{u}\, dv = W_T + W_V + W_M + W_{BF} \quad (4)$$

where $\mathbf{t}\cdot d\mathbf{u}$ is increment of work done by the traction force **t** during the increment of displacement d**u**, and $\mathbf{b}\cdot d\mathbf{u}$ is the increment of work done by the body force (gravity) vector **b** during the increment of displacement d**u**. For the two-dimensional solution of the foundation-soil system, these increments of work may be expressed in terms of the horizontal and vertical components of **t**, **b** and d**u** : $\mathbf{t}\cdot du = t_H du_H + t_V du_V$ and $\mathbf{b}\cdot d\mathbf{u} = \rho a_{grv} du_V$, where ρ is mass density and a_{grv} is acceleration due to gravity. For the foundation–soil system, $\sum W_e$ in Eq. (4) comprises (Fig. 9):

- $W_T = \int_{u_H} T\, du_H$; work done by the horizontal component of the external forces applied to the raft (u_H is horizontal displacement of the point of application of the horizontal load, T, at the center of the raft, point O in Fig. 9).
- $W_V = \int_{u_V} V\, du_V$; work done by the vertical component of the external forces applied to the raft, i.e. the weight of the pier and the raft (u_V is vertical displacement of the point of application of the vertical load $V = 860/82$ MN/m at the center of the raft, point O in Fig. 9).
- $W_M = \int_{\theta} M\, d\theta$; work done by the external moment $M =$ 30 T applied to the raft (Fig. 9).
- $W_{BF} = \int_v \int_{u_V} \rho a_{grv}\, du_V$; work done by the body gravity forces acting on the soil and inclusion masses (ρ is mass density and a_{grv} is acceleration due to gravity).

The numerical evaluation of the energies and works described above is based on the discrete counterparts of the corresponding expressions. Thus, integrals along the load path (i.e. $\int_u (\,) du$ or $\int_{\varepsilon} (\,) d\varepsilon$) and space-integrals (i.e. $\int_v (\,) dv$ for volume integrals or $\int_s (\,) ds$ for surface integrals) are replaced by summations. Volume integrals are tackled using summation over the whole set of finite elements assuming that stress, strain, and displacement fields (as well as mechanical properties) are constant over any given element.

6. Analysis of energy balance and damping

The results of the energy and damping computations are summarized in Tables 1–5. All calculations were conducted using digital data corresponding to both input and output of the 2D FE DYNAFLOW run which produced the results of Figs. 10 and 11. The meanings of the symbols for the energy contributions in Tables 1–4 and the expressions used to calculate these contributions were explained in the previous section. All contributions correspond to a rectangular foundation and have already been multiplied by the out-of-plane length of 82 m when appropriate. Three unloading–reloading loops were identified as follows by Points 1–9 shown in Figs. 10 and 11:

First loop: Maximum horizontal displacement, $u_m =$ 0.12 m (Points 123)
Second loop: Maximum horizontal displacement, $u_m = 0.34$ m (Points 456)
Third loop: Maximum horizontal displacement, $u_m =$ 0.55 m (Points 789).

Table 2
Internal energy dissipated/stored

Loop	u_m (m)	W_g (MN m)	W_c (MN m)	W_{ier} (MN m)	W_{iei} (MN m)	W_{el} (MN m)	W_{tip} (MN m)	ΣW_i (MN m)
123	0.12	37.6	143.0	17.2	0.3	1.8	0.3	200.2
456	0.34	183.1	530.7	66.0	4.5	14.6	1.2	800.1
789	0.55	256.5	674.1	722.3	29.6	12.5	12.4	1707.4

Table 3
Comparison between external and internal energies

Loop	u_m (m)	ΣW_e (MN m)	ΣW_i (MN m)	$\Sigma W_e/\Sigma W_i$
123	0.12	173.0	200.2	0.87
456	0.34	824.5	800.1	1.03
789	0.55	1645.3	1707.4	0.96

While the starting point of each loop is well defined, this is not true for the ending point as the first and second loops are not closed. Therefore, a criterion of equal maximum horizontal displacement was used in Fig. 10, with the values of displacement as listed above. For example, the first loop starts at Point 1 (tip of the loop) and ends at Point 3 (not a tip of any loop), with both Points 1 and 3 corresponding to the same displacement of 0.12 m. The same beginning and end loading steps were then used to define the corresponding beginning and end of the loop in Fig. 11.

Table 1 gives for each loop, the external energies associated with the horizontal force, T, moment, M, and vertical force, V. In all three loops, the contribution of the horizontal force T, W_T, was much larger than the rocking and vertical contributions. The contribution of V, W_V, is shown in parenthesis, as there is considerable uncertainty about this value, computed assuming that V is constant and always located at the center point of the raft. For completeness, Table 1 also has a column for the contributions W_{BF} of the vertical movements of the weights of the soil and inclusion elements; these could not be calculated because the node displacements were generally not available. It is believed that the values of W_{BF} were small. The last column of Table 1 shows the sum of contributions of the external loads, with and without including W_V.

Table 2 shows the internal energies dissipated or stored in the soil gravel and clay layers, interface elements under the raft and at the sides of the inclusions, stored elastically in the inclusions themselves, and dissipated at the tip elements under the inclusions. Most of these energies increased as the displacement of the loop increased, as expected. In general, most of the energy dissipation took place in the soil, except for the third loop where almost half of the energy was dissipated by sliding along the interface elements under the raft (as shown by the high value of W_{ier} in the table for this loop).

Table 4
Percentage contributions of different parts of the system to total internal energy

Part	Loop 123 ($u_m = 0.12$ m)	Loop 456 ($u_m = 0.34$ m)	Loop 789 ($u_m = 0.55$ m)
Gravel, W_g	18.8	22.9	15.0
Clay, W_c	71.5	66.4	39.6
Interface raft, W_{ier}	8.6	8.2	42.3
Interface inclusions, W_{iei}	0.1	0.6	1.7
Elastic energy inclusions, W_{el}	0.9	1.8	0.7
Inclusion tips, W_{tip}	0.1	0.1	0.7
TOTAL	100	100	100

Table 5
Equivalent damping ratios (%) of external loads

	Loop 123 ($u_m = 0.12$ m)	Loop 456 ($u_m = 0.34$ m)	Loop 789 ($u_m = 0.55$ m)
Horizontal Force–Displacement			
(a) From FE loop	42.0	46.8	59.1
(b) From monotonic curve and Masing criterion	24.6	29.8	23.5
Rocking Moment–Rotation			
(a) From FE loop	31.2	44.1	32.2
(b) From monotonic curve and Masing criterion	12.1	24.5	29.4

Table 3 verifies the global energy balance between internal and external energies. For the second and third loops, the agreement is excellent (within 5%), while for the first loop, the difference is 13%. This greater error is attributed to: (i) use of every fifth loading step in the energy calculations, and (ii) neglecting the term W_V corresponding to the work done by the vertical force V. Both potential sources of error are relatively more important for this smaller first loop than for the other two loops.

Table 4 breaks down the contributions of the various parts of the system to the global energy dissipation. That is, the table shows how much of the combined energy inside the horizontal force–displacement and rocking moment–rotation loops in Figs. 10 and 11, is dissipated or stored in the various soil, structural and interface parts. Table 4 is expressed in percentages. For the first two loops, two thirds of the energy was dissipated in the clay, with most of the rest dissipated in the gravel. The contribution of sliding under the raft for these two loops (W_{ier}) was less than 10%. On the other hand, for the third and largest loop, sliding under the raft was almost half of the total, with the clay and gravel soils contributing the other half. This is consistent with the very large damping ratio (almost 60%) associated with this loop in the horizontal force–displacement plot (Fig. 10 and Table 5), as well as with the shape of this loop, which exhibits large plateaus at the ends of both unloading and reloading branches. Another important conclusion from Table 4 is that the contact surfaces around the inclusions, represented by the sum of terms W_{iei} and W_{tip}, contributed less than 3% of the total internal energy dissipated or

stored. This result was used to eliminate the interface elements around the inclusions in subsequent 3D FE analyses conducted as part of the bridge project, thus simplifying the 3D models and increasing convergence speed significantly. An additional piece of information not included in Table 4, but calculated by the authors, is that out of the 15.0–22.9% of the total energy dissipated in the gravel, about half was dissipated in work associated with volumetric strains. That is, approximately 10% of the total energy dissipated was related to volumetric changes in the gravel layer during drained unloading–reloading. On the other hand, the whole contribution of the clay soil to energy dissipation in Table 4 was associated with shearing of the soil, as no volumetric changes were allowed.

Table 5 lists the equivalent damping ratios calculated for the three loops of Figs. 10 and 11. To define the elastic energy triangle needed for this calculation, the end point of the loop was used (e.g. Point 3 for the first loop in both Figs. 10 and 11). This table also includes the dampings computed from the corresponding monotonic backbone curves assuming Masing criterion. All damping ratios from the horizontal force–displacement loops are very large and they increase with u_m from 42 to 59%. This very high damping for the third loop was clearly associated with the large amount of sliding taking place during application of large displacements up to $u_m = 0.55$ m (see high W_{ier} in Table 2). The damping ratios from the rocking moment–rotation loops, while still large (31–44%) are somewhat smaller than the horizontal force–displacement ones. It is also interesting that in the third loop, the damping for rocking moment–rotation is relatively small, again confirming that sliding was the controlling factor for the 59% damping ratio listed in the table for the corresponding horizontal force–displacement loop. All damping ratios computed using Masing in Table 5 are significantly smaller than the ones obtained from the FE run, both for horizontal force–displacement and rocking moment–rotation. For horizontal force–displacement, these Masing dampings are in fact quite similar for the three loops (24–30%), consistent with the fact that the backbone curve for the large loop in Fig. 10 does not suggest failure, while the loop itself does.

The results of the 2D FE run in Table 5 would seem to suggest that the use of the Masing criterion is always conservative. However, this conclusion is quite sensitive to two aspects of the FE run reported herein: the specific stress–strain constitutive relation(s) used for the soil, and the specific loading condition used in the run. Other 2D FE runs conducted in the bridge project showed a better agreement between damping ratios obtained from the loops and those using Masing. Therefore, the systematic use of the Masing criterion for the foundation as part of the dynamic analyses of the bridge was based on the conclusion that this assumption is either realistic or conservative. Another consideration relevant to the validity of the Masing criterion is the height of the lever arm, $h = 30$ m, utilized in the results presented herein and related to the heights of the piers in the Rion-Antirion Bridge (Fig. 6). Additional 2D FE runs conducted with significantly higher values of h (not shown here), revealed high rotations and potential uplift of the foundation raft. After uplift occurred, use of the Masing criterion overestimated the damping ratio and hence was unconservative. While these much larger values of h and of foundation rotation do not apply to the actual conditions of the Rion-Antirion Bridge, the results again indicate the need to exercise caution. That is, the results of Table 5 should not be automatically assumed to be valid for other systems and seismic loading conditions, and the validity of the Masing criterion as an engineering approximation should be independently verified using tools similar to those described in this paper.

7. Conclusions

Main conclusions of these energy and hysteretic damping calculations from this 2D FE run using program DYNAFLOW are:

1. The calculations indicate reasonable balance between the internal and external energies associated with each of the three unloading–reloading loops, thus allowing identification of the contributions of the various components of the system to the total hysteretic energy dissipated jointly by the horizontal force and rocking moment acting on the foundation.
2. For foundation cyclic lateral displacements up to 0.34 m, about 90% of the total energy was dissipated in the two soil layers, mostly in the clay, with only about 8% dissipated by horizontal sliding along the interface elements under the raft. The combined contributions to total energy dissipation of the rest of the system (interfaces along inclusions and inclusion tips, and elastic energy changes in inclusions) were less than 2–3% in these two loops. This last result allowed better planning of 3D FE analyses conducted as part of the bridge project (not included here), in terms of not including the interfaces around the inclusions. This simplified the FE model and improved convergence speed.
3. When the foundation cyclic lateral displacement was increased to 0.55 m, the contribution of horizontal sliding along the interface elements under the raft jumped from 8 to 42% of the total, while that of the two soil layers decreased from 90 to 55%. The rest of the system again contributed only about 3% to total energy dissipation in this loop. The great importance of horizontal sliding suggested by those energy calculations for this loop, is consistent with the very significant plateaus observed in the two branches of the horizontal

force–displacement loop at foundation level. It is also consistent with the role of plastic hinge assigned in the design to the raft-gravel interface.

4. At foundation level, all equivalent damping ratios associated with the horizontal force–displacement loops were very large, increasing with the displacement of the loop and ranging from 42 to 59%. This last, very large value of damping was clearly associated with the sliding taking place between raft and gravel. The damping ratios from the rocking moment–rotation loops were somewhat smaller (31–44%), and they did not clearly increase with the displacement of the loop, consistent with the fact that much of the energy was dissipated at large displacements through cyclic horizontal sliding rather than rotation of the foundation.
5. The foundation equivalent damping ratios computed using the Masing criterion from the FE-calculated monotonic horizontal force–displacement and rocking moment–rotation curves, were significantly smaller than those obtained from the areas of the corresponding loops. For horizontal force–displacement, the range of damping ratios using Masing was 24–30% compared to 42–59% obtained from the loops. For rocking moment–rotation, the range of damping ratios using Masing was 12–29% compared to 31–44% obtained from the loops. These results, in conjunction with other 2D FE results, indicated that the use of Masing criterion for the seismic analyses of the Rion-Antirion Bridge was either realistic or conservative. However, these and other studies indicated that for other systems and seismic loading conditions the use of the Masing criterion may be unconservative. Factors identified as having significant influence on the validity of the Masing assumption were the soil stress–strain relation and the possibility of foundation uplift.

Acknowledgements

The authors are grateful to Gefyra Kinopraxia (Contractor of the project) and to Buckland & Taylor Ltd. (Checker of the project) for their permission to publish this paper. The authors also wish to thank Mr Jean-Paul Teyssandier of Gefyra Kinopraxia and Dr Peter Taylor of Buckland & Taylor Ltd. for their coordination, technical assistance and other contributions to the work discussed in the paper.

References

[1] Teyssandier JP, Combault J, Pecker A. Rion Antirion: le pont qui défie les séismes. La Recherche 2000;334:42–6.
[2] Teyssandier JP. Corynthian crossing. Civil Engng ASCE 2002; 72(10):42–9.
[3] Combault J, Morand P, Pecker A. Structural response of the Rion Antirion Bridge. Proceedings of the 12th World Conference on Earthquake Engineering. Auckland, Australia; 2000.
[4] Pecker A. Capacity design principles for shallow foundation in seismic areas. Keynote lecture. Proceedings of the 11th European Conference on Earthquake Engineering. Paris, France; 1998.
[5] Salençon J. Calcul à la rupture et analyse limite. Presses de l'Ecole Nationale des Ponts et Chaussées; 1983.
[6] Pecker A, Salençon J. Ground reinforcement in seismic areas. Proceedings of the XI Panamerican Conference on Soil Mechanics and Geotechnical Engineering. Iguaçu, Brazil; 1999.
[7] Pecker A. Le pont de Rion-Antirion: fiabilite et conception parasismique des foundations. In: Delage P, Habib P, De Gennaro V, editors. La sécurité des grands ouvrages. Hommage à Pierre Londe. Presses de l'Ecole Nationale des Ponts et Chaussées; 2000. p. 21–37.
[8] Crémer C, Pecker A, Davenne L. Cyclic macro-element of soil-structure interaction: material and geometrical nonlinearities. Int J Numer Anal Methods Geomech 2001;25(13):1257–84.
[9] Masing G. Eigenspannungen und Verfestigung beim Messing. Proceedings of the 2nd International Congress for Applied Mechanics; 1926. p. 332–335.
[10] Iwan WD. On a class of models for the yielding behavior of continuous and composite systems. J Appl Mech 1967;34:612–7.
[11] Prevost JH. Mathematical modelling of monotonic and cyclic undrained clay behavior. Int J Numer Anal Methods Geomech 1977;1(2):195–216.
[12] Geodynamique et Structure. 2D finite element analyses of a reinforced soil. Report GDS00045; 1998.
[13] Prevost JH. Plasticity theory for soil stress-strain behavior. J Engng Mech Division—ASCE 1978;104(5):1177–94.
[14] Prevost JH. A simple plasticity theory for frictional cohesionless soils. Soil Dyn Earthquake Engng 1985;4(1):9–17.
[15] Popescu R, Prevost JH. Centrifuge validation of a numerical model for dynamic soil liquefaction. Soil Dyn Earthquake Engng 1993;12(2): 73–90.
[16] Prevost JH. DYNAFLOW—A finite element analysis program for the static and transient response of linear and nonlinear two- and three-dimensional systems. Department of Civil Engineering, Princeton University; 1981.
[17] Dobry R, Zeghal M, Mavroeidis G. Global energy and damping calculations for unloading–reloading of foundation using results of DYNAFLOW 2D FE runs. Report No. B&T/003/Rev.0; 1999.